

# Journal of Biomedical Optics

[SPIEDigitalLibrary.org/jbo](http://SPIEDigitalLibrary.org/jbo)

## **Electric field Monte Carlo simulation of focused stimulated emission depletion beam, radially and azimuthally polarized beams for *in vivo* deep bioimaging**

Fuhong Cai  
Sailing He

# Electric field Monte Carlo simulation of focused stimulated emission depletion beam, radially and azimuthally polarized beams for *in vivo* deep bioimaging

Fuhong Cai<sup>a</sup> and Sailing He<sup>a,b,\*</sup>

<sup>a</sup>Zhejiang University, JORCEP, Centre for Optical and Electromagnetic Research, Zhejiang Key Laboratory of Sensing Technologies, Hangzhou 310058, China

<sup>b</sup>Royal Institute of Technology, Department of Electromagnetic Engineering, 100 44 Stockholm, Sweden

**Abstract.** An electric field Monte Carlo method is used to study the focal spot of a stimulated emission depletion (STED) beam, radially and azimuthally polarized beams in a turbid medium as a function of the scattering coefficient. To consider the diffraction of light of the wave nature, the wavefront is decomposed into a set of secondary spherical subwaves according to the Huygens principle. From the simulation results, we can find that the STED beam can still form a doughnut focal spot inside the turbid medium. These simulation results are important for the feasibility study of STED microscopy for *in vivo* deep bioimaging. Similarly, the focal spot for an azimuthally polarized beam can also keep a doughnut spot at the focal plane in a turbid medium.

© 2014 Society of Photo-Optical Instrumentation Engineers (SPIE) [DOI: [10.1117/1.JBO.19.1.011022](https://doi.org/10.1117/1.JBO.19.1.011022)]

Keywords: biomedical optics; Monte Carlo; vectorial field; scattering.

Paper 130295SSR received Apr. 30, 2013; revised manuscript received Oct. 5, 2013; accepted for publication Jan. 2, 2014; published online Jan. 24, 2014.

## 1 Introduction

Laser scanning microscopy (LSM) is a useful tool for bioimaging. Due to the diffraction limit of light, a traditional LSM cannot give a fine detailed image of a subcell structure. However, by using a deexcitation beam with a focal spot of doughnut shape, the so-called stimulated emission depletion (STED) microscopy<sup>1</sup> can give a super-resolution beyond the diffraction limit. By using a vortex phase plate to modulate a circularly polarized light, a light spot of doughnut shape can appear at the focal plane. This spatial phase-modulated light is usually called as an STED beam. Recently, STED microscopy has been applied to the surface layer of a living mouse brain with a resolution of about 67 nm.<sup>2</sup> The radially and azimuthally polarized beams also have the potential for super-resolution<sup>3</sup> bioimaging. Unlike a linearly or circularly polarized light, the polarization direction of a radially or azimuthally polarized beam is a function of the position at the wavefront at a fixed time. The focal spot of an STED beam, radially and azimuthally polarized beams in a transparent medium can be studied by using the vectorial diffraction theory.<sup>4</sup> In order to analyze the performance of the *in vivo* bioimaging microscopy, a method which can study the impact of the disorder of the turbid medium on the focal spot inside the biosample is desired. For example, if the doughnut focal spot cannot be formed inside a turbid medium, the STED microscopy cannot be applied to deep *in vivo* bioimaging. However, the vectorial diffraction theory cannot be directly applied to a highly scattering medium. In the present paper, we introduce a framework based on an electric field Monte Carlo<sup>5</sup> (EMC) method to simulate an STED beam in a turbid medium by taking into account the phase and coherent

interferences (which are not considered in a traditional Monte Carlo method). Benefiting from the new framework, the focal spot of a radially or azimuthally polarized optical beam can also be studied in a highly scattering tissue. To the best of our knowledge, no study has been reported before on the focal spot of these important beams in a turbid medium.

## 2 Method

Monte Carlo (MC) simulation is a good method for solving numerically the radiative transfer equation<sup>6</sup> and only the optical intensity (without the phase information) is considered in a traditional MC simulation. Thus, a traditional MC simulation cannot be utilized to study the propagation of the vectorial electric field in a turbid medium, such as the formation of the optical focal spot (of doughnut shape), which is due to the coherence properties of an optical beam (or STED beam/azimuthally polarized beam). Electric field Monte Carlo (EMC) simulation is an improved method, which can simulate the multiple scattering and absorption of the vectorial electric field in a turbid medium.<sup>5,7,8</sup> In EMC simulation, the sampling method for the free path between consecutive scattering events is the same as that in a traditional MC method. Unlike a traditional MC, as the electric field is scattered by the scattering spheres in a turbid medium, the Mie scattering theory [instead of the Henyey–Greenstein function used in a traditional MC (Ref. 6)] is applied to sample the scattering direction and change the polarization direction and phase of the wave packet correspondingly.<sup>5</sup> In our study, an EMC simulation framework is developed to simulate the focal spot inside a turbid medium. An aplanatic lens (AL) system is utilized as the focal objective

\*Address all correspondence to: Sailing He, E-mail: [sailing@kth.se](mailto:sailing@kth.se)

in the simulation. The entrance pupil of the AL is assumed to be uniformly illuminated by an optical wave of finite size with its propagation direction  $s$  parallel to the axis of the AL system, as shown in Fig. 1. To simplify the discussion, all aberrations are ignored and thus the wavefront in the image plane is a perfect "focal sphere."<sup>9,10</sup> The sine condition  $h = f \times \sin \theta$  can be applied to trace the wave packet<sup>5</sup> refracted by the AL system.<sup>10</sup> To consider the diffraction in the EMC simulation, each point of the wavefront in the image plane can be described as a source for the secondary spherical subwave according to the Huygens principle. In particular, for the AL system,  $V(\theta, \varphi)$  is defined as

$$V(\vartheta, \varphi) = \begin{bmatrix} 1 + (\cos \vartheta - 1) \cos^2 \varphi & (\cos \vartheta - 1) \cos \varphi \sin \varphi & -\sin \vartheta \cos \varphi \\ (\cos \vartheta - 1) \cos \varphi \sin \varphi & 1 + (\cos \vartheta - 1) \sin^2 \varphi & -\sin \vartheta \sin \varphi \\ \sin \vartheta \cos \varphi & \sin \vartheta \sin \varphi & \cos \vartheta \end{bmatrix}, \quad (1)$$

where  $\vartheta$  and  $\varphi$  are the deflection angle and azimuthal angle of the propagation direction of the secondary spherical subwave in the image plane and  $[P_x, P_y, P_z]$  is the unit polarization vector of the incident wave packet before the AL. As the incident wave packet passes through the AL, its polarization unit vector is updated as  $V(\vartheta, \varphi) \times [P_x, P_y, P_z]'$ . The details about Eq. (1) can be found in Refs. 4, 9, and 11.

As the secondary spherical subwave enters the turbid medium, it will undergo Mie scattering. In our simulation, the complex electric field vector of the secondary spherical subwave can be described as:  $\mathbf{E}_0 = e_1 \mathbf{m} + e_2 \mathbf{n}$ , where  $\mathbf{m}$  and  $\mathbf{n}$  are the unit polarization vectors in the directions of the parallel and perpendicular components.<sup>5</sup> As the wave propagates a free path  $l$  in the direction  $s$ , it would be scattered according to Mie theory

$$\begin{pmatrix} m' \\ n' \\ s' \end{pmatrix} = \begin{pmatrix} \cos \theta \cos \phi & \cos \theta \sin \phi & -\sin \theta \\ -\sin \phi & \cos \phi & 0 \\ \sin \theta \cos \phi & \sin \theta \sin \phi & \cos \theta \end{pmatrix} \begin{pmatrix} m \\ n \\ s \end{pmatrix}. \quad (2)$$

After the scattering, the complex electrical field is modified as

$$\begin{pmatrix} e_1' \\ e_2' \end{pmatrix} = [F(\theta, \phi)]^{-1/2} \begin{pmatrix} S_2 \cos \phi & S_2 \sin \phi \\ -S_1 \sin \phi & S_1 \cos \phi \end{pmatrix} \begin{pmatrix} e_1 \\ e_2 \end{pmatrix}, \quad (3)$$

where  $F(\theta, \phi)$  is defined as the light intensity normalization factor.<sup>12</sup> The details about the propagation of wave in a turbid

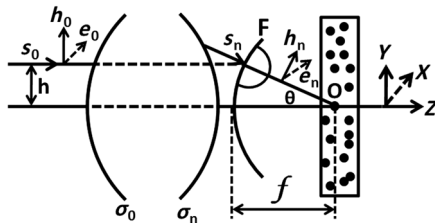


**Fig. 1** The diagram for the incident electrical field and the aplanatic lens (AL) system. The AL system is equivalent to a perfect lens and a focused spherical wavefront is formed when the incident wave is refracted by the AL system.

medium can be found in Ref. 5. The absorption is assumed to be 0 in the present study.

In our study, the wavelength of the incident optical electrical field is 1000 nm. The focal spot is 500  $\mu\text{m}$  deep inside a planar slab. In Secs. 2.1 and 2.2, the planar slab is considered as a transparent medium, whose scattering coefficient is  $0.0001 \text{ cm}^{-1}$  and the refractive index of the medium is 1.0. The work medium of the AL is air in these two subsections. For other sections, the EMC simulation is performed in a turbid medium. The scattering spherical particles inside the turbid medium have a diameter of 1  $\mu\text{m}$ , and the refractive indexes of the spherical particles and background medium are 1.518 and 1.33, respectively. To simplify the discussion, a water immersion AL is selected as the objective. This way, the mismatch of the refractive index between the work medium of the AL and the background medium can be ignored in the EMC simulation. Since the speed of the EMC simulation is very slow, we use a graphics processing unit to accelerate the EMC simulation.<sup>12</sup>

## 2.1 Cell Size of Voxel in EMC Simulation

As described in Ref. 5, the size of the voxel in the simulated medium should be small enough to resolve the interference pattern. However, as the voxel size gets smaller, the simulation time would get longer. In order to select a suitable voxel size, we simulated two focal spots of a linearly polarized (along the  $x$ -axis) beam by running the EMC simulation with meshes of 10 and 1 nm voxel sizes, and the results are shown in Figs. 2(a) and 2(b), respectively. Herein, the numerical aperture (NA) of the AL system is 0.92 and the EMC simulation only records the electrical field in a 1000 nm square region at the focal plane ( $XY$  plane). Thus, only a part of the secondary spherical subwaves, which can reach the 1000 nm square region, are traced in the EMC simulation.

In Fig. 2(c), the normalized optical intensity curves along the black line in Figs. 2(a) and 2(b) agree well with each other. The relative error/mismatch between these two curves for 10 and 1 nm voxel meshes is  $<2\%$ , as shown in the inset of Fig. 2(c). From the above results, one sees that the 10 nm voxel size is small enough to obtain a fine interference pattern. Hence, in our further study below, the simulated medium is meshed by a 10 nm voxel size.

## 2.2 Validation of the Focal Spot Derived From EMC Simulation

In order to verify the simulated focal spot in our study, a series of EMC simulations are performed with different values of NA. The radius of the Airy spot at the focal plane ( $XY$  plane) is compared with the diffraction limit  $r = 0.61 \lambda/\text{NA}$ . Herein, the refractive index and scattering coefficient of the turbid medium are set as 1.0 and  $0.0001 \text{ cm}^{-1}$ , respectively. The incident optical wave is of circular polarization. The results are shown in Fig. 3. There is some small relative error which is due to the statistical error of the EMC simulation and the finite voxel size (10 nm). Hence, we have validated the EMC simulation for the calculation of the focal spot.

## 2.3 Simplification of the Secondary Spherical Subwave

As described in Sec. 2.1, when the medium is transparent, the focal spot is the result of interference of many secondary

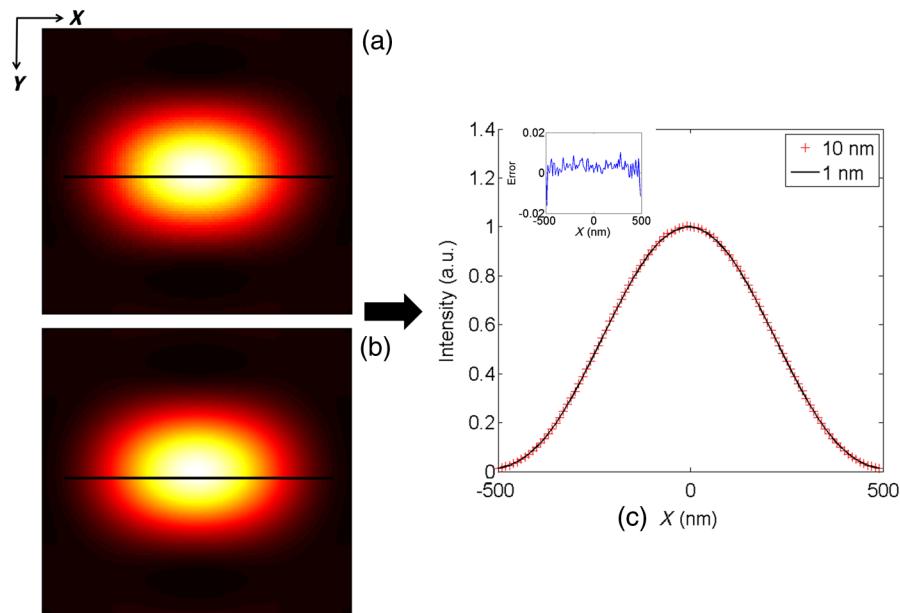


**Fig. 2** (a) and (b) depict the focal spots which are obtained from the EMC simulation with meshes of 10 and 1 nm voxel size, respectively. (c) The normalized optical intensity curves from our EMC simulations with meshes of 10 and 1 nm voxel size, respectively. Inset shows the relative error of these two curves. The statistical errors are due to the nature of the EMC simulation.

spherical subwaves which can reach the region of interest (ROI) around the focal spot. The part of the secondary spherical subwaves which can reach directly the ROI in a transparent medium is called “effective secondary spherical subwaves.” However, in a turbid medium, part of non-effective secondary spherical subwaves may reach the ROI due to the multiple scattering. Theoretically speaking, the EMC simulation needs to trace all the secondary spherical subwaves, instead of only the effective secondary spherical subwaves, to obtain an accurate result in a turbid medium. However, this way the computing time would greatly increase. As described in Ref. 7, the optical interference pattern is predominantly stemmed from unscattered light. Therefore, we can assume (approximately) that only “effective secondary spherical subwaves” will contribute to the focal spot in a turbid medium.

Two simulations are performed to verify this hypothesis. For both the simulations, the scattering coefficient is  $68 \text{ cm}^{-1}$  and the NA is 0.51. The ROI-1 is a 2000 nm square region in the focal plane (XY plane) for the first EMC simulation. In the

second EMC simulation, the size of ROI-2 is 4000 nm. In the first/second simulations, the simulated secondary subwaves would cover ROI-1/2. In the second simulation, part of the secondary spherical subwaves, which are not effective secondary spherical subwaves, will reach the focal spot through multiple scattering. If our hypothesis is wrong, the scattered secondary spherical subwaves will affect significantly the simulation results of focal spot and these two simulation results would have a big difference. Two simulated intensity curves of focal spot are shown in Fig. 4(a) and the relative error is shown in Fig. 4(b). The main part of these two curves matches well, while the random error is prominent at the fringe of the curves. The relatively large random error at the fringe may arise from the scattered secondary spherical subwaves. However, the optical intensity at the fringe of the curves is extremely small, indicating that the simulated focal spot’s intensity and the full width at half maximum (FWHM) of the focal spot are valid by only tracing the “effective secondary spherical subwaves” in a turbid medium. This way the simulation time can be greatly reduced. In the next section, the EMC simulation is utilized to study the STED beam, radially and azimuthally polarized beams and only “effective secondary spherical subwaves” are traced.

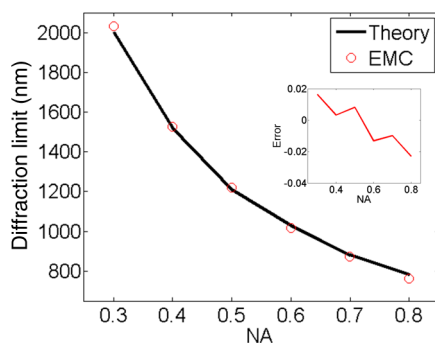


**Fig. 3** The radius of an Airy spot at the focal plane (XY-plane) obtained from our EMC simulation and the diffraction theory. The inset shows the relative error between the results obtained from our EMC simulation and the diffraction theory.

### 3 Simulation Results

In STED microscopy, a vortex phase plate is used to modulate the phase of the incident wave to generate the doughnut focal spot. In order to involve the vortex phase plate in the EMC, the complex amplitude of the incident wave, which passes through  $(x_0, y_0, z_0)$  at the entrance pupil, is multiplied by  $e^{i\varphi_0}$ , where  $\tan(\varphi_0) = y_0/x_0$ . For radially and azimuthally polarized waves, the unit polarization vector  $[P_x, P_y, P_z]$  of the incident wave can be defined as  $[\cos \varphi_0, \sin \varphi_0, 0]$  and  $[-\sin \varphi_0, \cos \varphi_0, 0]$ , respectively. The NA of the AL system is 0.92 throughout this section.

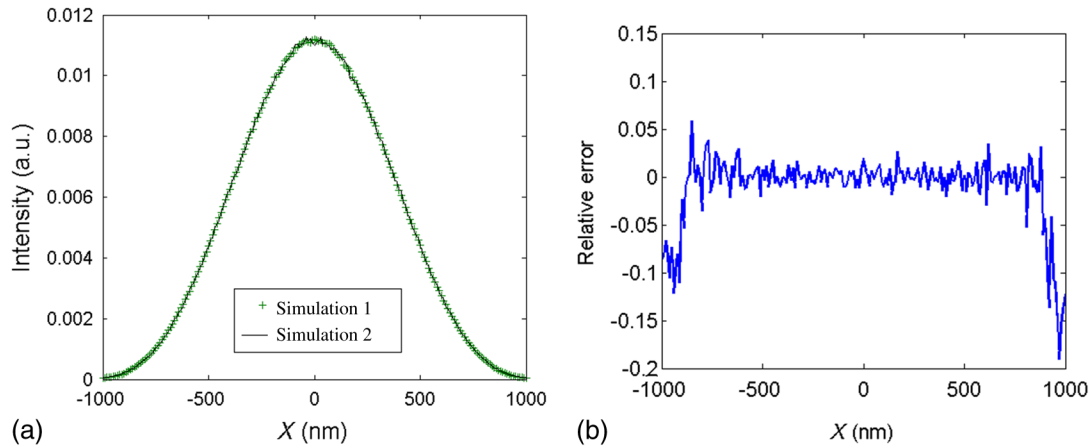


**Fig. 4** (a) The simulated optical intensity curves at the focal spot with “the first and second simulations” described in Sec. 2.3. (b) The relative error for the two curves shown in (a).

### 3.1 Intensity Distribution of Focal Spot Inside Turbid Medium

Figures 5(a)–5(d) illustrate the patterns of the STED focal spots. Even in the scattering medium, the focal spots can still keep a doughnut shape. However, the profile of the doughnut spot is broadened as the scattering coefficient gets larger. Figures 5(e)–5(h) illustrate the focal spots of a radially polarized beam. Unlike the STED beam, the peak intensity of the focal spot of a radially polarized beam is at the center of the focal

pattern (and thus cannot be used for an STED microscopy). As shown in Figs. 5(e) and 5(g), the focal spot pattern is significantly enlarged when the scattering coefficient increases from 10 to 40  $\text{cm}^{-1}$ . These results indicate that the focal spot profile for a radially polarized beam is more sensitive to the scattering as compared to an STED beam, an azimuthally polarized beam, or a linearly polarized beam.<sup>7</sup> One possible explanation for this phenomenon is as follows. Both the changes of the polarization and the phase can affect the focal spot. As the light scatters within a turbid medium, its polarization vector

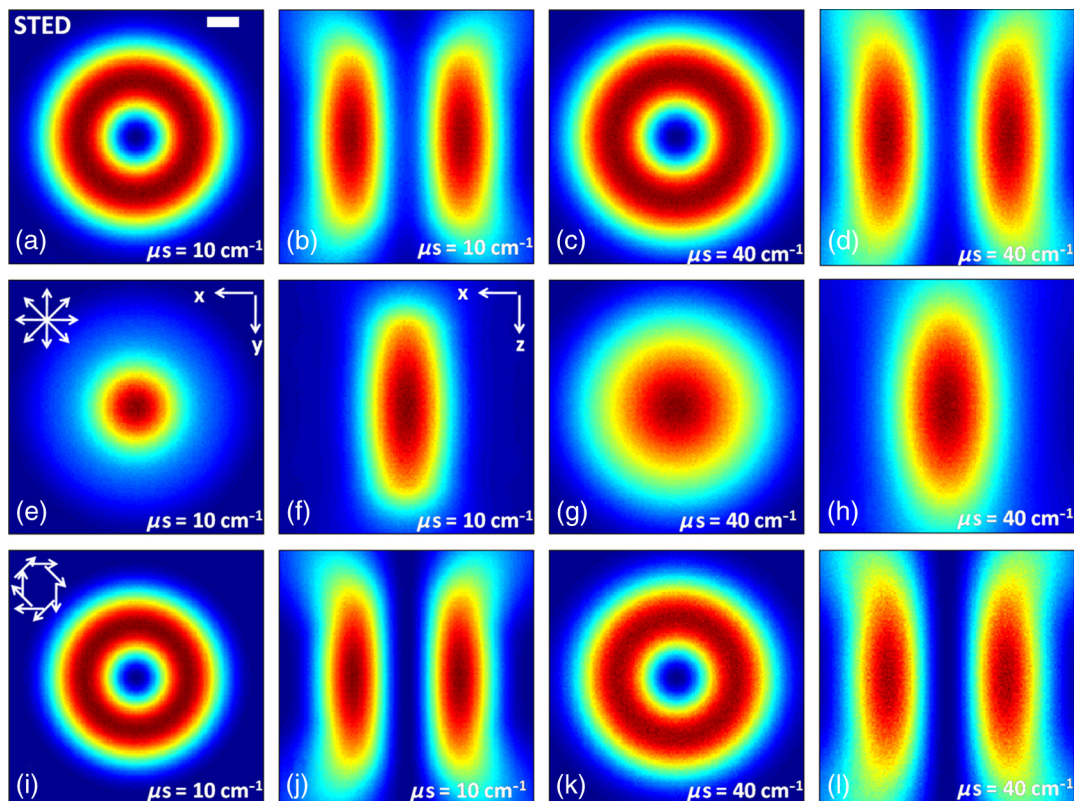


**Fig. 5** The optical intensity distribution at the focal spot inside a turbid medium. The first to third rows depict the intensity distribution of an STED beam, radially and azimuthally polarized beams. The first and third columns depict the intensity distribution at the focal spot in the horizontal ( $XY$ ) plane and the second and fourth columns depict the intensity distribution at the focal spot in the longitudinal ( $XZ$ ) plane. To describe the dimension of the focal spots in Fig. 5, a scale bar (200 nm) is shown in (a).

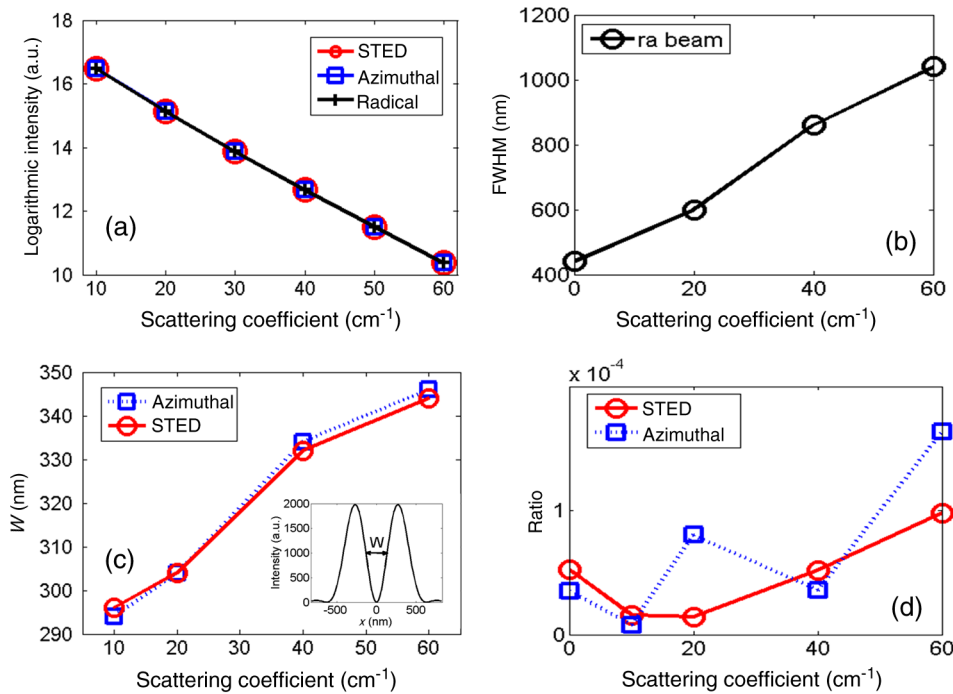


**Fig. 6** Scattering dependence of the focal spot. (a) The intensity of the focal spot inside the turbid medium. (b) Full width at half maximum of the focal spot for a radially polarized beam. (c) The dark region's width of the doughnut focal spot for an azimuthally polarized beam and an STED beam. (d) The intensity ratio between the middle nadir and the peak in the doughnut beam.

would be deflected to other directions. As we know, same polarization is a key requirement for the constructive interference. Compared with a linearly polarized beam, a radially polarized beam has the most abundant elements of polarization vectors. Hence, as the scattering gets larger, the probability for constructive interference in the focal spot of a radially polarized beam is larger than that of a linearly polarized beam. Therefore, in the focal spot of a radially polarized beam, the intensity decay rate from the middle to the fringe becomes much slower and the FWHM for a radially polarized beam increases much more quickly as the scattering coefficient increases. The focal spots of an azimuthally polarized beam are shown in Figs. 5(i)–5(l). Similar to the STED beam, the focal spots of the azimuthally polarized beam are also doughnut-shaped. A quantitative analysis for the focal spots of an STED beam, radially and azimuthally polarized beams will be given in Sec. 3.2.

### 3.2 Quantitative Results for the Intensity and Size of the Focal Spot Inside a Turbid Medium

As expected, due to the strong scattering in a turbid medium, the optical intensity of an STED focal spot is sharply attenuated as the scattering coefficient increases. The simulation results are shown in Fig. 6(a). Since the super-resolution of an STED microscopy is achieved via stimulated emission, which is a non-linear optical effect and required a high optical intensity density, the decay of the optical intensity of the doughnut spot may be not conducive to the application of the STED microscopy in deep tissue imaging. The scattering-dependent intensity of a focal spot for a radially or azimuthally polarized wave is exactly the same as the STED spot, which are also shown in Fig. 6(a). Figures 6(b) and 6(c) give a more explicit quantitative analysis

for the broadening of the focal spot. In Fig. 6(b), the FWHM of the radially polarized beam substantially increases as the scattering coefficient increases. For the doughnut-shaped spot, the dark component is critical to achieve a better resolution. The width of the dark region is defined as 'W' as shown in the inset of Fig. 6(c), and the dark region is extended when the scattering coefficient increases. Based on the above results, the performance of the STED microscopy would be deteriorated in a scattering medium. Another important characteristic of the doughnut-shaped spot is the intensity ratio between the middle nadir and the peak in a doughnut beam. In theory, the ratio is 0 in a transparent medium. However, due to the statistical error of the Monte Carlo simulation, the ratio is about  $5.0 \times 10^{-5}$  when the scattering coefficient is  $0.0001 \text{ cm}^{-1}$ . As the scattering coefficient gets larger, the ratio increases but is still  $< 2.0 \times 10^{-4}$  for both the azimuthally polarized beam and the STED beam. The result is shown in Fig. 6(d), which further illustrates that the doughnut-shaped spot can be well kept in a turbid medium. Note that the intensity of the middle spot in the STED beam and the azimuthally polarized beam should be zero theoretically. However, Monte Carlo simulation is a statistical method, and thus its simulation data would have some statistical error in a turbid medium. Consequently, the intensity ratio is very small but fluctuates a bit in Fig. 6(d).

## 4 Conclusion

An electric field Monte Carlo framework has been developed and implemented to characterize the focal spot in a turbid medium. Since the polarization direction and the phase at each point in the incident wave can be modified arbitrarily, we have used our simulation method to study the STED beam, radially and azimuthally polarized beams in a turbid medium. As expected, the optical intensity is greatly attenuated

as the scattering coefficient increases. Due to the multiple scattering, the size of the focal spot also gets larger. The EMC simulation can give more quantitative results for the attenuated intensity and enlarged size of the focal spot. Another important result is that even in a turbid medium, the STED beam can still form a doughnut focal beam. This result reveals the feasibility of the STED microscopy for *in vivo* deep bioimaging. However, due to the large attenuation of the light intensity in a scattering medium, a laser system with a larger power is needed to achieve an *in vivo* super-resolution in the STED microscopy. The azimuthally polarized beam has similar characteristics as the STED beam. For a radially polarized beam, the FWHM is greatly enlarged as the scattering coefficient increases, indicating its poor resolution for deep tissue bioimaging.

### Acknowledgments

This work is supported by the National Nature Science Foundation of China (No. 61008052), the Science and Technology Department of Zhejiang Province (No. 2010R50007), and Brain-Bridge project (ZJU-TU/e and Philips Research collaboration).

### References

1. S. W. Hell and J. Wichmann, "Breaking the diffraction resolution limit by stimulated emission: stimulated-emission-depletion fluorescence microscopy," *Opt. Lett.* **19**(11), 780–782 (1994).
2. S. Berning et al., "Nanoscopy in a living mouse brain," *Science* **335**(6068), 551 (2012).
3. R. Dorn, S. Quabis, and G. Leuchs, "Sharper focus for a radially polarized light beam," *Phys. Rev. Lett.* **91**(23), 233901 (2003).
4. X. Hao et al., "Effects of polarization on the de-excitation dark focal spot in STED microscopy," *J. Opt.* **12**(11), 115707 (2010).
5. M. Xu, "Electric field Monte Carlo simulation of polarized light propagation in turbid media," *Opt. Express* **12**(26), 6530–6539 (2004).
6. L. Wang, S. L. Jacques, and L. Zheng, "MCML—Monte Carlo modeling of light transport in multi-layered tissues," *Comput. Methods Programs Biomed.* **47**(2), 131–146 (1995).
7. C. K. Hayakawa et al., "Amplitude and phase of tightly focused laser beams in turbid media," *Phys. Rev. Lett.* **103**(4), 043903 (2009).
8. C. K. Hayakawa, E. O. Potma, and V. Venugopalan, "Electric field Monte Carlo simulations of focal field distributions produced by tightly focused laser beams in tissues," *Biomed. Opt. Express* **2**(2), 278–290 (2011).
9. E. Wolf, "Electromagnetic diffraction in optical systems. I. An integral representation of the image field," *Proc. R. Soc. London Ser. A* **253**(1274), 349–357 (1959).
10. B. Richards and E. Wolf, "Electromagnetic diffraction in optical systems II. Structure of the image field in an aplanatic system," *Proc. R. Soc. London Ser. A* **253**(1274), 358–379 (1959).
11. F. Cai, J. Yu, and S. He, "Vectorial electric field Monte Carlo simulations for focused laser beams (800 nm–2220 nm) in a biological sample," *Prog. Electromagn. Res.* **142**, 667–681 (2013).
12. Y. Wang et al., "GPU accelerated electric field Monte Carlo simulation of light propagation in turbid media using a finite-size beam model," *Opt. Express* **20**(15), 16618–16630 (2012).

**Fuhong Cai** is a postdoctoral fellow at the Center for Optical and Electromagnetic Research, Zhejiang University. His main research activities are focused on bio-photonics, including setting up optical imaging systems and simulations for photon migration in turbid mediums.

**Sailing He** is currently the director for the Joint Research Center of Photonics of the Royal Institute of Technology in Sweden, Lund University in Sweden and Zhejiang University, China. He is a fellow of OSA, IEEE, and SPIE.